Biophysical Journal Volume 103 November 2012 2000–2010

A Basic Set of Homeostatic Controller Motifs

T. Drengstig,[†] I. W. Jolma,[‡] X. Y. Ni,[‡] K. Thorsen,[†] X. M. Xu,[‡] and P. Ruoff[‡*]
[†]Department of Electrical Engineering and Computer Science and [‡]Centre for Organelle Research, University of Stavanger, Stavanger, Norway

ABSTRACT Adaptation and homeostasis are essential properties of all living systems. However, our knowledge about the reaction kinetic mechanisms leading to robust homeostatic behavior in the presence of environmental perturbations is still poor. Here, we describe, and provide physiological examples of, a set of two-component controller motifs that show robust homeostasis. This basic set of controller motifs, which can be considered as complete, divides into two operational work modes, termed as inflow and outflow control. We show how controller combinations within a cell can integrate uptake and metabolization of a homeostatic controlled species and how pathways can be activated and lead to the formation of alternative products, as observed, for example, in the change of fermentation products by microorganisms when the supply of the carbon source is altered. The antagonistic character of hormonal control systems can be understood by a combination of inflow and outflow controllers.

INTRODUCTION

Homeostasis is the concept that describes the coordinated physiological processes maintaining most of the steady states in organisms (1–3). Homeostasis does not necessarily imply a lack of change, but may include time-dependent behavior such as set-point changes or oscillatory responses (1,2). Alternative terminologies, such as predictive homeostasis (4,5), rheostasis (5,6), or allostasis (5,7), have been suggested to address these dynamic aspects of homeostatic control, and to emphasize the connection to adaptive and anticipatory functions of circadian rhythms together with the occurrence of orchestrated set-point changes. Common to all these homeostasis-related concepts is the presence of coordinated responses to maintain internal cellular and organismic stability (8).

An important aspect of adaptive or homeostatic systems is their robustness (9–14), i.e., their ability to maintain functionality in the presence of various uncontrollable environmental disturbances. From a control-engineering perspective, the concept of integral control leads to robust perfect adaptation (15). The use of integral control in homeostatic biological systems (16) was discussed by Saunders and colleagues (17,18) and its use in robust perfect adaptation of reaction kinetic networks has been demonstrated by Yi et al. (19) and others (20–23). We showed that the presence of zero-order kinetics in the degradation/inhibition of the controller molecule in two-component negative feedback loops is a way to achieve integral control and robust homeostasis (21). As a continuation of our previous work (21), we present here, with physiological examples, a complete set of two-component homeostatic controller motifs and their division into inflow and outflow controllers. We identify parameters that influence the accuracy of the controllers and determine how hierarchical homeostatic behaviors of combined controllers can lead to multiple steady-state levels corresponding to the different controllers' set points. We show how controller combinations can integrate uptake and assimilation within a cell and may lead to pathway switching in terms of outflow control, forming new products. Also, dysfunctional behavior, such as integral windup (15), has been found in single and combined controllers, and its possible biological significance in relation to disease is mentioned.

COMPUTATIONAL METHODS

Rate equations were solved numerically using MATLAB/SIMULINK and FORTRAN. For details, see the Supporting Material. To make notations simpler, concentrations of compounds are denoted by compound names without square brackets. Concentrations and rate constants are given in arbitrary units (a.u.) unless stated otherwise.

RESULTS

Basic set of homeostatic controller motifs

The motifs we consider here consist of negative feedback loops with two species, A and E, both of which are being formed and turned over. In control theoretic terms, A is called the controlled variable, which is kept at a homeostatic level, whereas species E is the manipulated variable (MV). Fig. 1 *a* shows the (complete) set of eight two-component molecular representations of negative feedback loops between A and E (hereby called motifs or controllers). The systematic construction of the eight motifs is given in the Supporting Material.

It should be noted that the negative feedback loops alone are not sufficient to provide homeostasis. Ni et al. (21) found that to achieve perturbation-independent homeostasis, the

Submitted January 1, 2012, and accepted for publication September 25, 2012.

*Correspondence: peter.ruoff@uis.no

Editor: Andre Levchenko.

0006-3495/12/11/2000/11 $2.00

http://dx.doi.org/10.1016/j.bpj.2012.09.033

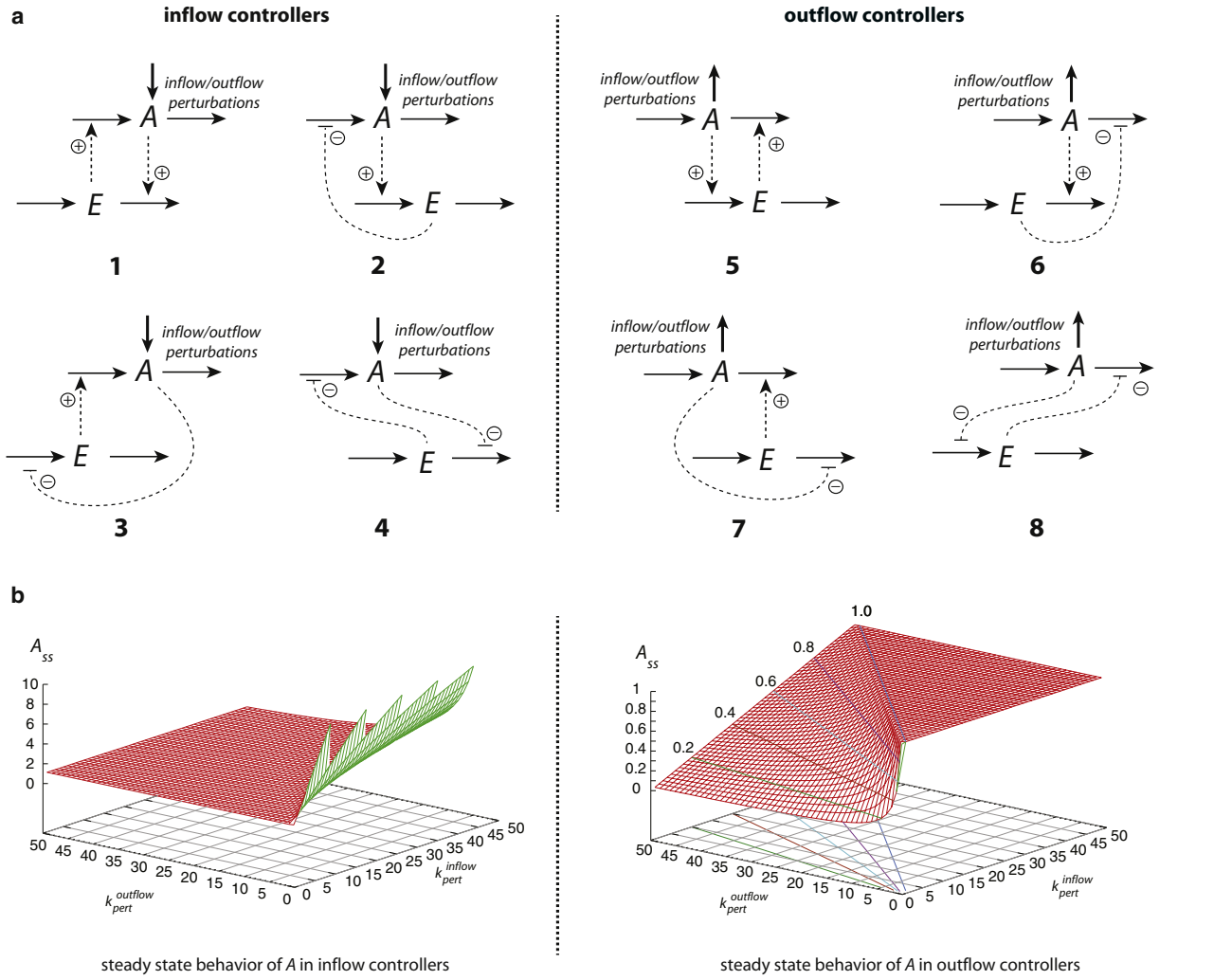

FIGURE 1 A complete set of two-component homeostatic controller motifs. (*a*) The motifs fall into two operational classes termed inflow and outflow controllers (for definition, see main text). Each motif is able to show robust homeostasis in A when the MV, E, is subject to removal by zero-order kinetics. (*b*) Figures show the steady-state values of A for inflow and outflow controllers as a function of k_{pert}^{inflow} and $k_{pert}^{outflow}$, respectively, with $A_{set}^{in} = A_{set}^{out} = 1$. Typically, the homeostatic behavior of all inflow controllers breaks down when inflow perturbations become dominant (A_{ss} levels rise above A_{set} ; *left*), whereas for outflow controllers, homeostasis breakdown is observed when outflow perturbations from A become dominant (A_{ss} levels decrease below A_{set} ; *right*). At these breakdowns, the compensatory flux, j_A (Eq. 1), is zero, which defines the lower borders of the controller homeostatic regions.

removal of E by zero-order kinetics (due to an enzyme, E_{set}) is a sufficient condition. We will show below that under these zero-order kinetic conditions, integral control is operational, where the level of E is proportional to the integrated error between A and set point A_{set}.

Four of the motifs in Fig. 1 were published previously (21), and Yi et al. (19) gave the first example of motif 2 exhibiting robust homeostasis by including zero-order removal of the MV, but without mentioning the importance of zero-order kinetics in obtaining integral control. Here, we describe four additional motifs, which makes the set complete.

Closer inspection of the motifs shows that the set divides equally into two operational classes recognized in our previous work (21) and termed inflow and outflow controllers. However, inflow controllers are here redefined as maintaining homeostasis by adding A to the system from an internal or environmental source, whereas outflow controllers maintain homeostasis by removing A from the system.

The dynamics of A can be written as

$$\dot{A} = k_{pert}^{inflow} - k_{pert}^{outflow} \times A \pm j_A, \qquad (1)$$

where k_{pert}^{inflow} and $k_{pert}^{outflow}$ are parameters related to uncontrolled inflow/outflow perturbations, and j_A is the E-mediated compensatory flux, which adds A to or removes it from the system by inflow or outflow controllers, respectively.

As emphasized previously (21), the homeostatic behavior of inflow controllers breaks down when there are large uncontrolled inflows, whereas outflow controllers lose their homeostatic behavior in the presence of large uncontrolled outflows. At these breakdowns, the E-mediated compensatory fluxes (j_A) of added or removed A become zero, and

the steady-state behavior in A becomes $A_{ss} = k_{pert}^{inflow}/k_{pert}^{outflow}$, as indicated in Fig. 1 *b*.

As discussed below, the controller breakdown related to $j_A \rightarrow 0$ represents the lower (zero) j_A border in the controller homeostatic regions, whereas another, upper j_A border in the controller homeostatic regions appears when, due to kinetics or capacity factors, the j_As reach an upper limit.

Set-point determination and controller accuracy

The motifs in Fig. 1 *a* show four different ways in which A can influence E: 1), by activating the removal of E (motifs 1 and 6); 2), by activating the synthesis of E (motifs 2 and 5); 3), by inhibiting the synthesis of E (motifs 3 and 8); and 4), by inhibiting the removal of E (motifs 4 and 7).

The expression for the set point, A_{set}, for each controller motif is determined by the steady-state condition of the MV, E, by how A influences E, and by assuming that E is removed by an enzyme, E_{set}, with zero-order kinetics. As an example, the following equations show the determination of A_{set} for inflow controller 3, where A is inhibiting E:

$$\dot{E} = k_s^E \times \frac{K_I^A}{K_I^A + A} - \frac{V_{max}^{E_{set}} \times E}{K_M^{E_{set}} + E}. \quad (2)$$

When $K_M^{E_{set}} \ll E$, the steady-state condition in E leads to the expression for the theoretical set point of inflow controller 3:

$$A_{set} = \frac{k_s^E \times K_I^A}{V_{max}^{E_{set}}} - K_I^A. \quad (3)$$

If the value of $K_M^{E_{set}}$ is comparable to the level of E, a difference between the theoretical set point (Eq. 3) and the steady-state value of A (A_{ss}) is introduced, which can be related to the controller's accuracy, α, defined by $\alpha = A_{set} - A_{ss}$.

We note that homeostatic breakdown of a controller due to large inflow/outflow changes, as indicated in Fig. 1 *b*, and a controller's accuracy are therefore two distinct features (see also Fig. S9).

To identify the mathematical expression for the accuracy, α, we compare the rate equations of the individual controllers with the structure of a standard integral control law from control engineering (15), i.e., $\dot{E} = K_i \times (A_{set} - A_{meas})$, where K_i is called the integral gain, A_{meas} is the measurement signal, and A_{set} is the theoretical set point. For inflow controller 3 (Eq. 2), we get the integral control law

$$\dot{E} = \underbrace{\frac{V_{max}^{E_{set}}}{K_I^A + A}}_{K_i} \times \left(\underbrace{\frac{k_s^E \times K_I^A}{V_{max}^{E_{set}}} - K_I^A}_{A_{set}} - \underbrace{\left(f(E) \times \left(K_I^A + A\right) - K_I^A\right)}_{A_{meas}} \right), \quad (4)$$

with $f(E) = E/(K_M^{E_{set}} + E)$. Note that the measurement signal, A_{meas}, is generally a nonlinear function of A, i.e., $A_{meas} = g(A)$. In terms of biochemical processes in cells, A_{meas} reflects the overall signal-transduction events originating from A and leading to a change in E. For controllers 3, 4, 7, and 8, the integral gain, K_i, varies with the level of A. In control theoretical terms this is referred to as gain scheduling (15).

The accuracy, $\alpha = A_{set} - A_{ss}$, of inflow controller 3 can be calculated by finding A_{ss} from the steady-state condition for E using Eq. 2 or Eq. 4.

Table 1 groups the controllers in accordance with conditions 1–4 (defined above) of how A affects E and shows that each group has its own expression for A_{set}, A_{meas}, K_i, and α. Rate equations of the controller motifs are given in the Supporting Material.

As shown in Table 1, two parameters determine the accuracy of a controller: the Michaelis constant, $K_M^{E_{set}}$ (through $f(E)$), from the degradation of E by E_{set} (present in all controllers); and the inhibition constant, K_I^A (A inhibiting the formation or removal of E), for controllers 3, 4, 7, and 8.

Although the accuracy, α, of each controller is perfect $(\alpha \approx 0)$ when $f(E) \approx 1$, i.e., $K_M^{E_{set}} \ll E$ and $K_I^A \ll A$ (only for controller 3, 4, 7, and 8), the α values differ for each of the four cases in Table 1 when $K_M^{E_{set}}$ cannot be ignored in comparison with E. A graphical presentation of the accuracy of the controllers as a function of E, $K_M^{E_{set}}$, and K_I^A is given in Fig. S10. For motifs 1, 3, 6, and 8, α has large unbounded negative values when E becomes small, whereas for the remaining motifs 2, 4, 5, and 7, α increases with decreasing E, with $\alpha = A_{set}$ being an upper bound.

TABLE 1 Expressions for accuracy, α, set point, A_{set}, measurement function, A_{meas}, and integral gain, K_i, for each controller motif

Motif	A_{set}, A_{meas}	K_i, α
1, 6	$A_{set} = \frac{k_s^E}{V_{max}^{E_{set}}}$	$K_i = V_{max}^{E_{set}}$
	$A_{meas} = f(E) \times A$ †	$\alpha = A_{set} - \frac{A_{set}}{f(E)}$ †
2, 5	$A_{set} = \frac{V_{max}^{E_{set}}}{k_s^E}$	$K_i = -k_s^E \times f(E)$†
	$A_{meas} = \frac{A}{f(E)}$ †	$\alpha = A_{set} - A_{set} \times f(E)$†
3, 8	$A_{set} = \frac{k_s^E \times K_I^A}{V_{max}^{E_{set}}} - K_I^A$	$K_i = \frac{V_{max}^{E_{set}}}{K_I^A + A}$
	$A_{meas} = f(E) \times (K_I^A + A) - K_I^A$ †	$\alpha = A_{set} - \left(\frac{A_{set} + K_I^A}{f(E)} - K_I^A\right)$†
4, 7	$A_{set} = \frac{V_{max}^{E_{set}} \times K_I^A}{k_s^E} - K_I^A$	$K_i = -\frac{k_s^E}{(K_I^A + A)} \times f(E)$†
	$A_{meas} = \frac{(K_I^A + A)}{f(E)} - K_I^A$ †	$\alpha = A_{set} - ((A_{set} + K_I^A) \times f(E) - K_I^A)$

†$f(E) = \frac{E}{K_M^{E_{set}} + E}$.

Performance of individual controllers

We considered the question of what factors will influence the homeostatic regions when controllers have the same accuracies and set points.

If no restrictions are made on the concentrations in E and on the inflow/outflow compensatory fluxes, j_A, all eight controllers show identical regions of homeostasis, only limited by the lower j_A flux border of the controllers, as indicated in Fig. 1 *b*. However, differences in controller performances occur when the compensatory fluxes, j_A, become limited due to either different capacities of the different controllers to generate E or differences in the kinetics of the E-induced j_A fluxes.

To illustrate the influence of j_A limitation on homeostatic performance, we chose for each controller a set point of 2.0 a.u. and a maximum compensating flux of $j_{A,max} = 10$ a.u. To achieve this, the $V^{E_{tr}}_{max}$ parameters for controllers 1, 3, 5, and 7 were chosen such that $j_{A,max} = 10$ is obtained at a maximum level of $E_{max} = 20$, whereas for the E-inhibiting controllers, $j_{A,max} = 10$ is obtained when $E \to 0$. Note that the E-activated fluxes, j_A, in controllers 1, 3, 5, and 7 are first-order with respect to E, whereas the j_A fluxes due to E inhibition (controllers 2, 4, 6, and 8) show saturation kinetics, i.e., $j_A = j_{A,max} \times K_I^E/(K_I^E + E)$ (see derivation of j_A in the Supporting Material, Eq. S12). As will be shown below, these differences between E-activating and E-inhibiting j_A kinetics will lead to different controller performance.

When comparing A_{ss} levels between controllers, we found that all E-activating controllers (1, 3, 5, and 7) behaved practically identically, as did all E-inhibiting controllers (2, 4, 6, and 8). However, when comparing E-inhibiting controllers with E-activating controllers, the E-inhibiting controllers performed less well at low K_I^E values than did the E-activating controllers. As an example, Fig. 2 shows the steady-state values of A, E, and j_A for controllers 1 and 2 and controllers 5 and 6. E-activating controllers 1 and 5 (Fig. 2, *red*) can maintain their homeostatic steady states in A as long as $j_A < j_{A,max}$. Once $j_A \to j_{A,max} = 10$ the upper border of the homeostatic region is reached and homeostasis breaks down. For low K_I^E values, the j_A fluxes of E-inhibiting controllers 2 and 6 (Fig. 2, *blue*) are not large enough to compensate for the applied outflow perturbation, and their homeostatic performance is poor compared to the E-activating controllers. However, at larger K_I^E and $j_{A,max}$ values, the performance of the E-inhibiting controllers can match the performance of the E-activating controllers.

On the other hand, when the first-order kinetics with respect to E in the E-activating controllers is replaced by saturation kinetics, i.e., $j_A = j_{A,max} \times E/(K_a^E + E)$, then, as for the E-inhibiting controllers (Fig. 2), the homeostatic performance is dependent on the value of K_a^E and is limited

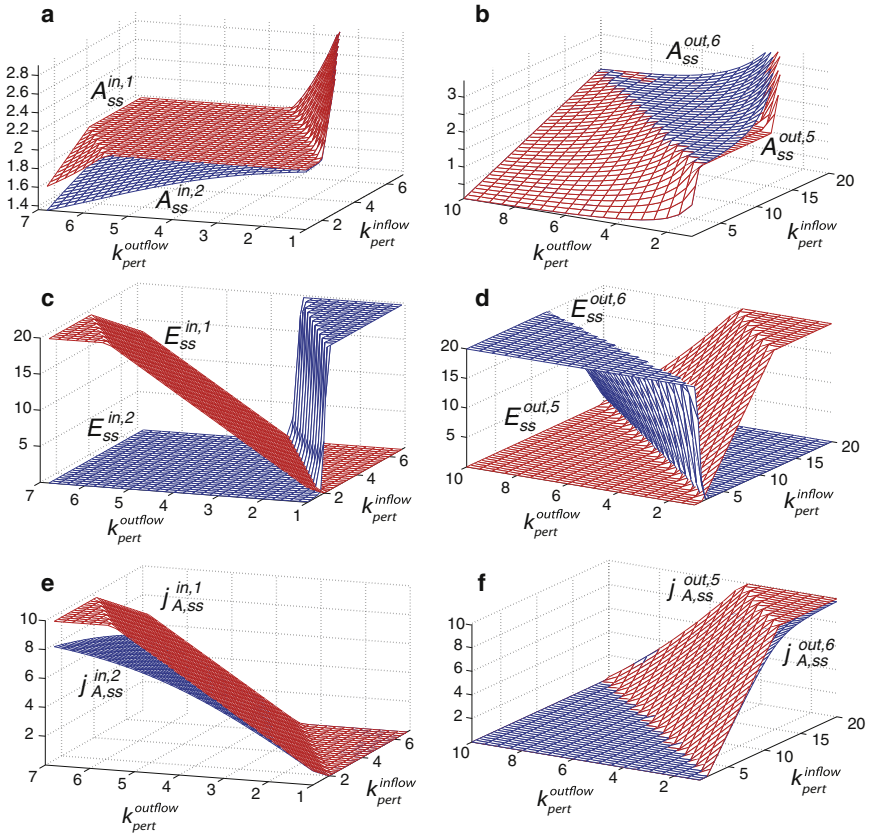

FIGURE 2 Controller comparisons. (*a*, *c*, and *e*) Behaviors of E-activating and E-inhibiting inflow controllers 1 and 2 with respect to the steady-state levels of A and E and the E-mediated inflow of A and j_A. Inflow controllers 3 and 4 show practically identical behaviors (data not shown). (*b*, *d*, and *f*) Behaviors of activating and inhibiting outflow controllers 5 and 6 with respect to the steady-state levels of A and E and the E-mediated outflow of A and j_A. Outflow controllers 7 and 8 show almost identical behavior (data not shown). See also Fig. S6 and Fig. S7 and the Supporting Material description of how j_A kinetics can influence controller performance.

by the maximum compensatory flux $j_{A,max}$ (see Supporting Material for derivation of j_A expression (Eq. S8) and details (Fig. S7)). Thus, the homeostatic performance of the controllers depends largely on the kinetics of the compensatory flux, j_A, and its limits and not on the negative feedback structure of the controller motif.

Controllers' hierarchical dominance

Many of the homeostatic control mechanisms that occur in higher organisms are mediated by hormones that often act as antagonistic pairs when exercising control on a particular compound (such as blood glucose). As inflow- and outflow-controller motifs can be identified as occurring as physiological antagonists (see Discussion), we investigated homeostatic performance by combining inflow- and outflow-controller motifs.

Fig. 3 shows an example of combined inflow/outflow controllers using controllers 1 and 5. The dashed lines refer to signal transduction originating from A and affecting MVs E_1 (controller 1) and E_5 (controller 5), which now have the functions of inflow and outflow transporters, respectively. See Combination of controllers, in the Supporting Material, for details.

For the combined inflow/outflow controllers we have three possible set-point combinations, i.e., $A^{in}_{set} < A^{out}_{set}$, $A^{in}_{set} = A^{out}_{set}$, and $A^{in}_{set} > A^{out}_{set}$. When combining solely inflow or solely outflow controllers, we get two additional combinations, i.e., $A^{in,i}_{set} > A^{in,j}_{set}$ and $A^{out,k}_{set} > A^{out,l}_{set}$, where i and j refer to inflow- and k and l to outflow-controller motifs. These possible controller combinations are described in more detail in the following sections.

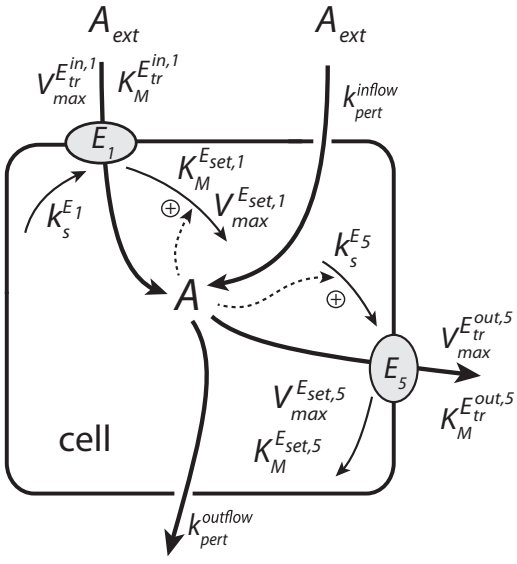

FIGURE 3 Combining inflow and outflow controllers. Reaction-kinetic representation of combining inflow controller 1 and outflow controller 5 (see Rate Equations S38–S40 in the Supporting Material). The inflow controller will add A when the outflow perturbation is larger than the inflow perturbation. In a similar way, the outflow controller will remove A when the inflow perturbation is larger than the outflow perturbation. In general, an inflow controller will not add any A unless the level of A is below A^{in}_{set}, and an outflow controller will not remove any A unless the level of A is above A^{out}_{set}.

For the sake of simplicity, we will not consider an upper j_A limit in the capacity of controllers that may lead to homeostatic breakdown, as shown in Fig. 2. However, in the Supporting Material, we give an example (Fig. S13) of how the overall region of homeostasis is the union of the homeostatic regions of the inflow/outflow controllers, with the upper j_A borders of the two controllers defining the limits of the overall homeostatic region. The lower j_A borders (Fig. 1 *b*) of both controllers merge and are embedded in the region of homeostasis.

Combination 1, $A^{in}_{set} < A^{out}_{set}$

Dependent on the inflow or outflow perturbations, the steady-state level of A will either end up at one of the set points or stay between the set points.

In the case where the inflow perturbation is dominating, the outflow controller will remove any excess of A until A^{out}_{set} is reached. When initial levels of A are lower than A^{in}_{set} (Fig. 4 *a*), the inflow controller is active until the A level has exceeded A^{in}_{set}. Although the inflow controller has become inactive, the dominating inflow perturbation will drive the level of A to A^{out}_{set}. A slight increase of A above A^{out}_{set} will activate the outflow controller and keep the A level at A^{out}_{set} (Fig. 4 *b*). When the initial level of A is above A^{out}_{set} (Fig. 4 *c*), the inflow controller is inactive and the outflow controller will drive A to A^{out}_{set} and keep it there.

If the outflow perturbation is dominant, the inflow controller will add A to the system and finally keep the level of A at A^{in}_{set}. If the level of A is below A^{in}_{set} (Fig. 4 *e*), the outflow controller is inactive, but the inflow controller will add sufficient A to the system to keep the level of A at A^{in}_{set} (Fig. 4 *f*). In the case where the initial A level is above A^{out}_{set} (Fig. 4 *g*), the outflow controller will be active until the level of A has sunken to A^{out}_{set}. Then the dominating outflow perturbation will drive the A level to A^{in}_{set}. Once the level of A is below A^{in}_{set}, the inflow controller will become active and keep the A level at A^{in}_{set}.

In case the inflow/outflow perturbations are such that the steady state of A lies between the upper and lower set points, the level of A will remain at this position, with both inflow and outflow controllers inactive (Fig. 4 *d*).

Fig. 4 *h* gives a graphical representation of the two homeostatic domains as a function of the inflow/outflow perturbations, k^{inflow}_{pert} and $k^{outflow}_{pert}$. The two homeostatic domains are separated by a transition zone, in which both controllers are inactive. The borders to the transition zone (Fig. 4 *h*, *dashed lines*) are described by two equations, compactly written as

$$k^{inflow}_{pert} = k^{outflow}_{pert} \times A^{in/out}_{set}, \quad (5)$$

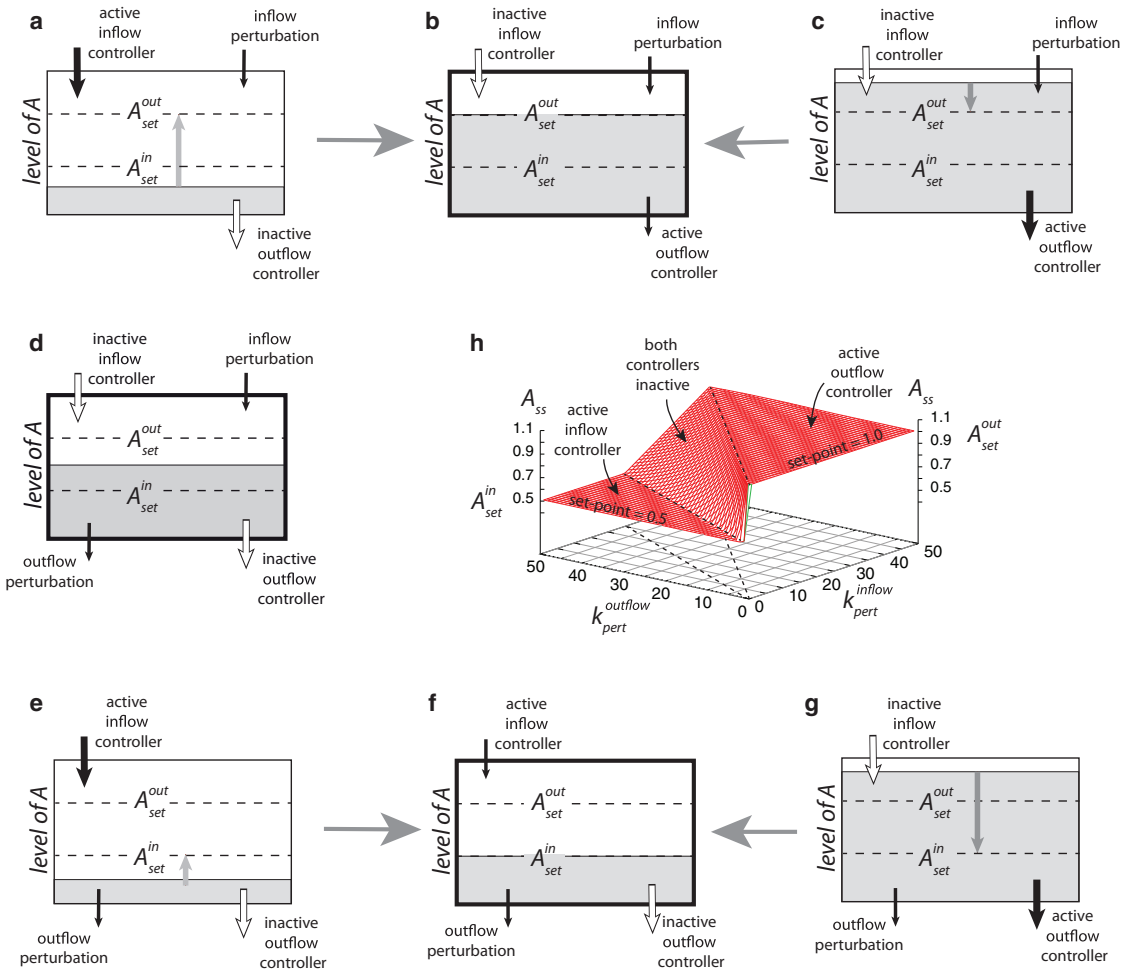

FIGURE 4 System behavior when combining an inflow and an outflow homeostatic controller such that $A^{in}_{set}<A^{out}_{set}$ using a simplified tank analogy. Black arrows indicate active controllers and active inflow/outflow perturbations, and white arrows indicate inactive controllers. The steady-state value of A as a function of k^{inflow}_{pert} and $k^{outflow}_{pert}$, with the three segments corresponding to the steady-state levels shown in *b*, *d*, and *f*, can be seen in the center row (*h*) The other panels represent transitional states. (*Upper row*) Tanks show how A settles to A^{out}_{set} (*b*) in the presence of a dominating inflow perturbation. (*Lower row*) Tanks show how A settles to A^{in}_{set} (*f*) in the presence of a dominating outflow perturbation. (*Middle row*) Both controllers become inactive when $A^{in}_{set}<A_{ss}<A^{out}_{set}$ (*d*). For modeling details, see Eqs. S39–S41 and Fig. S11 and Fig. S12.

where $A^{in/out}_{set}$ denotes either A^{in}_{set} or A^{out}_{set}. The lower dashed line in Fig. 4 *h* can be understood as the transitions occurring at different but constant $k^{outflow}_{pert}$ values when the inflow controller goes from an active to an inactive state during an increase in k^{inflow}_{pert}. At these transitions the concentration of A is A^{in}_{set}, but the contributions from both controllers to A (j_A in Eq. 1) have vanished. Thus, Eq. 5 (for A^{in}_{set}) can then be deduced from Eq. 1. In a similar way, Eq. 5 for A^{out}_{set} can be deduced for the upper dashed line.

Combination 2, $A^{in}_{set}=A^{out}_{set}$

In this case, the steady-state level of A will end up at the common set point (within the limits of the accuracy). Both controllers will in general be active and the level of controller activity (i.e., the fluxes of A being transported in and out) depends on the levels of inflow and outflow perturbations.

Combination 3, $A^{in}_{set}>A^{out}_{set}$

In this case, the steady-state level of A lies between A^{in}_{set} and A^{out}_{set} (Fig. S14), with both controllers working against each other. The inflow controller adds A to the system to increase the A level to A^{in}_{set}. At the same time the outflow controller removes A to reduce the level of A down to A^{out}_{set}. During this process, E_{in} and E_{out} values continually increase for controllers 1, 3, 5, and 7, where E activates the inflow to or outflow from A. For an example, see Fig. S15 *b*. Both controllers may eventually reach their maximum capacities (maximum E or j_A levels), leading to controller breakdown, similar to the case in Fig. 2 for individual controllers 1 and 5.

When controllers are of the inhibiting kind (motifs 2, 4, 6, and 8), E will become zero, leading to the least possible inhibition and to controller breakdown, as shown for controllers 2 and 6 in Fig. 2 (see also Fig. S19 *d*).

Although for this combination no distinct set points can be observed for different k_{pert}^{inflow} and $k_{pert}^{outflow}$ values (see Fig. S14), the location of the A steady state between A_{set}^{in} and A_{set}^{out} depends on the parameters of the individual controllers. For example, when the dominance of the outflow controller is very low ($V_{max}^{E_{tr}^{out}}$ is low relative to $V_{max}^{E_{tr}^{in}}$), then the inflow controller determines the steady state of A (see Fig. S14 *a*). By successively increasing the $V_{max}^{E_{tr}^{out}}$ of the outflow controller, the steady state in A changes gradually toward A_{set}^{out}, see Fig. S14 *c*.

Combination 4, $A_{set}^{in,i} > A_{set}^{in,j}$

Combining two inflow controllers, i and j (assuming a high uncontrolled outflow in A), controller i, with the higher set point, is active and determines the set point, whereas controller j, with the lower set point, is inactive (Fig. S17).

Combination 5, $A_{set}^{out,k} > A_{set}^{out,l}$

When combining two outflow controllers, k and l (assuming a high uncontrolled inflow in A), controller l, with the lower set point, will dominate and determine the A value. Controller k, with the higher set point, is inactive, because the level of A is lower than $A_{set}^{out,k}$ and there is no need for controller k to remove more A.

Activating pathways

Using Combination 1 between an inflow and an outflow controller, the activation of the outflow controller pathway is observed when an (uncontrolled) inflow of A into a cell becomes dominant. In Fig. 4 *f*, a sudden dominating inflow perturbation will lead to a change from inflow control to outflow control (Fig. 4 *b*) via the transition zone (Fig. 4 *d*). In addition, a change (increase) in the steady-state concentration of A from A_{set}^{in} to A_{set}^{out} will be observed. In terms of outflow control, two situations can be considered, one in which excess of A is transported out of the cell (excreted), as in Fig. 3, or one in which the excess of environmentally taken up A (environmental concentration of A is denoted A_{ext}) is transformed into one or several products within the cell by an overflow pathway (with flux j_2) (Fig. 5 *a*). In Fig. 5 *a*, A can enter the cell by an uncontrolled (diffusion-like) first-order mechanism with flux $k_{pert}^{inflow} \times A_{ext}$ and by inflow controller 1, where the manipulated variable E_1 plays the role of the transporter with set point $A_{set}^{in} = 1$. The overflow pathway is regulated by outflow-controller motif 5, where the manipulated variable E_5 plays the role of an enzyme converting A into another product. The overflow pathway has a set point of $A_{set}^{out} = 2$. In the absence of an uncontrolled inflow of A ($k_{pert}^{inflow} = 0$ in Fig. 5 *a*), the level of A is determined by inflow controller 1 with $A_{set}^{in} = 1$, and all A is directed into the essential pathway with flux j_1. Typically, for inflow controllers, transporter E_1 will deliver to the essential pathway only as much A as is needed (which may depend on environmental conditions). At these conditions, the overflow pathway is shut off. However, when an additional large inflow of A occurs, the concentration of A within the cell increases until the set point of the outflow controller is exceeded. At that stage, the outflow controller is activated and removes excess of A by enzyme E_5 with

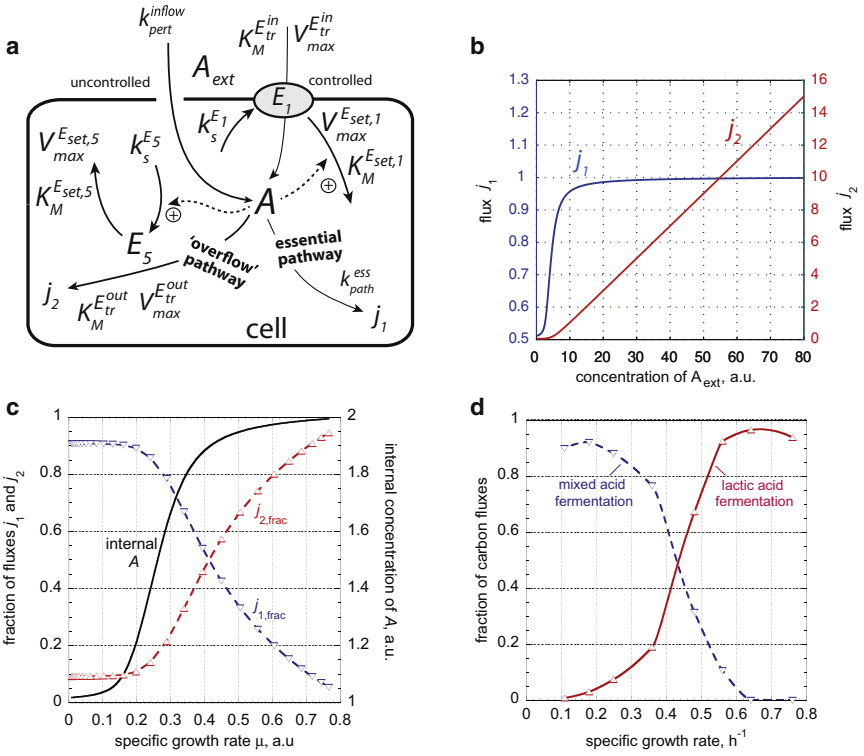

FIGURE 5 Illustration of pathway activation by a combination of inflow 1 and outflow 5 controllers. (*a*) Excess of A can be handled by a cell-internal overflow pathway with flux j_2. (*b*) Induction of the overflow pathway when a large inflow of A enters the cell, leading to an increase in fluxes j_1 and j_2. Rate-constant values are given in Activated pathways in the Supporting Material. (*c*) Calculated fractional fluxes $j_{1,frac}$ and $j_{2,frac}$ from *b* together with the internal concentration of A as a function of the specific growth rate, μ. (*d*) Experimentally observed shift of metabolic pathways in *Streptococcus lactis* from mixed-acid production at low growth rates to lactic acid production at high growth rates. Replotted from Fig. 4 *c* of Molenaar et al. (27).

flux j_2 while the level of A is kept at $A_{set}^{out} = 2$. Fig. 5 *b* shows the changes in j_1 and j_2 as a function of A_{ext}. At low A_{ext} levels, inflow controller 1 dominates, with $j_1 = k_{path}^{ess} \times A_{set}^{in}$ and $j_2 = 0$. With increasing inflow of A, due to an increased A_{ext}, the overflow pathway is activated and j_2 increases with increasing A_{ext}. With the change in set point from A_{set}^{in} to A_{set}^{out}, flux j_1 also increases and approaches $j_1 = k_{path}^{ess} \times A_{set}^{out}$.

Fig. 5 *c* shows the fractional fluxes, $j_{1,frac} = j_1/(j_1 + j_2)$ and $j_{2,frac} = j_2/(j_1 + j_2)$, as a function of the specific growth rate, μ, which is related to A_{ext} by Monod's equation for bacterial growth (24,25):

$$\mu = \mu_{max} \times \frac{A_{ext}}{K_s + A_{ext}}. \quad (6)$$

At low A_{ext} (and low growth rate), i.e., when there is a relatively high cell internal demand for A, inflow controller 1 supplies the necessary A flux needed by the essential pathway, keeping the internal level of A at A_{set}^{in}. At this stage, flux j_2 (and thereby $j_{2,frac}$) is low and $j_{1,frac}$ is close to 1, as shown in Fig. 5 *c*. With increasing A_{ext} levels (and increasing growth rates), the inflow of A (with rate constant k_{pert}^{inflow}) increases and the inflow controller is no longer able to maintain homeostasis. As a result, the internal A concentration increases until the set point of the outflow controller is reached (A_{set}^{out}).

In Fig. 5 *d*, an analogous behavior of fractional carbon fluxes in *Streptococcus lactis* (26,27) is shown, changing from mixed-acid fermentation at low growth rates to lactic acid fermentation at high growth rates. Although the phenomenon of metabolic shifting as shown in Fig. 5 *d* is still not fully understood (27), the concept of coupled inflow and outflow controllers may provide an explanation of how an alternative pathway could be activated in terms of homeostatic set-point switching.

DISCUSSION

Fig. 1 shows a basic set of two-component negative feedback motifs. Applying zero-order removal of the MV, E, by an enzyme, E_{set}, introduces integral control and transforms each of the negative-feedback mechanisms into robust homeostatic controllers. The $K_M^{E_{set}}$ values (and K_I^A values for some controllers) are related to controller accuracy, α (Table 1). The biological significance of these controller motifs is briefly discussed in the next sections.

Biological significance

We asked the question to what extent the controller motifs and their inflow/outflow and switching behaviors can be related to physiological observations. Due to space limitations, we focus here on a few examples concerning metal-ion homeostasis and hormonal systems and how degradation/inhibition mechanisms may be involved in set-point determination. Further descriptions and several other physiological examples are given in the Supporting Material.

Iron, heme, and metal-ion homeostasis

In *Arabidopsis*, IRT1 is the major high-affinity transporter for the uptake of iron and other metals. IRT1 has been found to be subject to an iron-induced turnover (28). Combining this with an IRT1-mediated uptake of iron, inflow controller motif 1 (Fig. 1 *a*), with IRT1 playing the role of E, appears to be a plausible candidate (see also Fig. S22). Further support for the presence of inflow-control-mediated metal-ion homeostasis comes from yeast studies, where inflow controller motifs can be identified (see Supporting Material). In these cases, metal-ion-mediated turnover of the various transporters by the ubiquitin-proteasome pathway has been implicated with respect to iron, zinc, and copper (29–31). The presence of an inflow controller motif for iron uptake by plants reflects the limited access plants have for iron, as under normal conditions iron in soil is present as little soluble iron(III)-oxide. To our knowledge, for higher plants, no outflow controller motif has been identified with respect to iron homeostasis.

Interestingly, in the case of yeast, there is evidence for an iron-outflow controller motif, where transcription factor Aft1p activates Cth2, which specifically downregulates mRNAs that encode proteins participating in iron-dependent and consuming processes (32) (Fig. S23).

With respect to mammalian iron homeostasis, inflow controller 1 and outflow controller 5 can be identified. At low and limiting iron concentrations, iron homeostasis can be described by inflow controller 1, where IRP2 (together with IRP1) plays the role of the MV, E, stabilizing mRNAs of iron-utilizing proteins by binding to iron-responsive elements (33) and activating the flow of iron into the cell by transferrin receptors (34,35). As iron levels increase, IRP2 becomes subject to an iron-dependent proteasomal degradation mediated by the F-box protein FBXL5, which becomes stabilized as iron concentrations increase (Fig. S20). At high iron concentrations active IRP levels are low due to the degradation of IRP2 by the proteasome (36,37) and the transformation of IRP1 to an aconitase (33). This allows controller motif 5 to take over by exporting iron out of the cell using the iron-induced transporter ferroportin, which corresponds to the MV. Ferroportin is regulated by binding to hepcidin, which leads to internalization and degradation of ferroportin (Fig. S21) (38). Thus, variations in iron concentration may lead to switching between inflow- and outflow-controller mechanisms (in analogy to Fig. 4) while maintaining iron homeostasis (36,37,39).

Heme, an iron-containing porphyrin is an important cofactor for many proteins and found to be under homeostatic control. Heme production has been found to be

inhibited by Rev-erbα (a transcriptional repressor) by inhibiting PGC-1, a key metabolic transcription factor (40). To obtain homeostatic control of heme, heme could either activate Rev-erbα (Fig. 1 *a*, *motif 2*) or inhibit Rev-erbα degradation/inhibition (Fig. 1 *a*, *motif 4*). Studies of a *Drosophila* homolog of Rev-erbα, E75, indicate that E75 binds to heme and leads to an increase in E75 stability (41), suggesting that inflow controller motif 4 is a possible candidate for the homeostatic regulation of heme in flies and maybe in mammals (Fig. S25). Interestingly, besides regulating heme homeostasis, Rev-erbα is also implicated in the coordination of the mammalian circadian clock, acting there as an inhibitor of BMAL1 (42,43), as well as in glucose homeostasis and energy metabolism (44), indicating a relationship between homeostatic and circadian control.

Homeostasis by hormonal control

Hormones play an essential part in the homeostasis of our bodies by controlling a variety of parameters such as iron, glucose, calcium, or potassium/sodium. Interestingly, hormonal control systems have an antagonistic organization and come generally in pairs. There has been made the argument that one (hormonal) controller would in principle be sufficient for providing homeostasis and not two (18). So, why have two? Using the control of blood glucose by insulin and glucagon as examples, Saunders and colleagues have investigated this question and provided a theory ('integral rein control') (18) of two antagonistic integral controllers that allow to make the system stable against relatively large perturbations in either direction. Studying various homeostatic systems controlled by hormones, it turns out that the two opposing hormonal controllers in 'integral rein control' appear closely related to the inflow and outflow controllers shown in Fig. 1. For example, control of blood glucose by insulin is closely related to outflow controller motif 5 (Fig. S35), whereas the homeostatic behavior provided by glucagon is that of inflow controller motif 3 (Fig. S36). The homeostatic regulation of iron in mammals by inflow controller 1 (with respect to IRT's) and outflow controller 5 (with respect to ferroportin) was already discussed above. See the Supporting Material for additional descriptions of hormone-regulated systems.

Controller limits

In most of our calculations, we assumed that controller performance was ideal, and not restricted by the controller capacity. However, due to the nature of inflow and outflow controllers, breakdowns occur when individual inflow or outflow controllers experience dominating inflow or outflow perturbations, respectively, as indicated in Fig. 1 *b*. This type of breakdown can be omitted when inflow and outflow controllers are combined in antagonistic pairs (Fig. 4). In addition, homeostatic control also breaks down when, for example, the amount of the MV, i.e., E, becomes limiting (Fig. 2). This type of homeostasis breakdown is related to a controller overload.

Controller breakdown also occurs when the compensating flux, j_A, becomes saturated and independent of E, for example, by a finite amount of an enzyme that catalyzes the production of A. In this case, the error between the set point of the (measured) value of A becomes constant and one observes a steady increase in E without decreasing the error (until saturation of E may occur). This type of behavior is referred to as integral windup in control engineering. Integral windup can also be observed in controller Combination 3, where the inflow and outflow controllers are of the E-activating type (controllers 1, 3, 5, 7). In this case, because $A_{set}^{in} > A_{set}^{out}$, both controllers remain active, as indicated in Fig. S15 *b*. Because there is a constant error between the actual value of A and the set points of the controllers in the case of both inflow and outflow controllers, in principle, E will increase without limits.

Biological systems of course have capacity limits, for example, on the amounts of proteins/enzymes produced. Thus, integral windup may represent a challenge with respect to the capacity demands biological controllers can tolerate, and it may lead to disease. The occurrence and significance of integral windup in biological systems is little explored and we wish to return to this subject later. The Supporting Material gives a brief description of when integral windup may occur in controller combinations under ideal conditions and with no capacity limits.

Since its introduction by Cannon, the concept of homeostasis addressing fixed set points has undergone several critical analyses (5,8). Set points were found to change, as in the case of body temperature, for example, which varies in a circadian manner, whereas during pathogen attack it rises and causes fever. These and other observations led to the concepts of predictive homeostasis (4) and rheostasis (6). In an approach to include anticipatory set-point changes, as well as controller overload, Sterling and Eyer introduced the term allostasis (7,8). The controller motifs presented here, together with their breakdown by molecular mechanisms, may provide tools to further investigate conditions related to the limits of homeostatic regulation (8).

CONCLUSIONS

We have presented a basic set of controller motifs that can show robust homeostasis, but we have also identified several causes for controller breakdown. For some of these motifs, we have identified their presence in physiological situations, but the role of isolated motifs should be viewed critically, as homeostatic controllers are embedded in interconnected networks from which new properties may emerge. The controller motifs presented here can be regarded as basic building blocks to provide homeostatic and adaptive behaviors.

SUPPORTING MATERIAL

Thirty-six figures, 53 rate equations, details of the computational methods, and references (45–78) are available at http://www.biophysj.org/biophysj/supplemental/S0006-3495(12)01074-0.

This research was financed in part by grants from the Norwegian Research Council to I.W.J. (167087/V40) and to X.Y.N. (183085/S10).

REFERENCES

1. Cannon, W. B. 1939. The Wisdom of the Body, 2nd ed. Norton, New York.
2. Hughes, G. M. 1964. Homeostasis and Feedback Mechanisms. Academic Press, New York.
3. Langley, L. L., editor. 1973. Homeostasis. Origins of the Concept. Dowden, Hutchinson & Ross, Stroudsbourg, PA.
4. Moore-Ede, M. C. 1986. Physiology of the circadian timing system: predictive versus reactive homeostasis. *Am. J. Physiol.* 250:R737–R752.
5. Schulkin, J. 2004. Allostasis, Homeostasis and the Costs of Physiological Adaptation. Cambridge University Press, Cambridge, MA.
6. Mrosovsky, N. 1990. Rheostasis. The Physiology of Change. Oxford University Press, New York.
7. Sterling, P., and J. Eyer. 1988. Allostasis: a new paradigm to explain arousal pathology. *In* Handbook of Life Stress, Cognition and Health. S. Fisher, and J. Reason, editors. John Wiley & Sons, New York. 629–649.
8. Schulkin, J. 2004. Rethinking Homeostasis. Allostatic Regulation in Physiology and Pathophysiology. MIT Press, Cambridge, MA.
9. Barkai, N., and S. Leibler. 1997. Robustness in simple biochemical networks. *Nature.* 387:913–917.
10. Alon, U., M. G. Surette, …, S. Leibler. 1999. Robustness in bacterial chemotaxis. *Nature.* 397:168–171.
11. Carlson, J. M., and J. Doyle. 2002. Complexity and robustness. *Proc. Natl. Acad. Sci. USA.* 99 (*Suppl 1*):2538–2545.
12. Yang, Q., P. A. Lindahl, and J. J. Morgan. 2003. Dynamic responses of protein homeostatic regulatory mechanisms to perturbations from steady state. *J. Theor. Biol.* 222:407–423.
13. Stelling, J., U. Sauer, …, J. Doyle. 2004. Robustness of cellular functions. *Cell.* 118:675–685.
14. Kitano, H. 2007. Towards a theory of biological robustness. *Mol. Syst. Biol.* 3:137.
15. Wilkie, J., M. Johnson, and K. Reza. 2002. Control Engineering. An Introductory Course. Palgrave, New York.
16. Milsum, J. H. 1966. Biological Control Systems Analysis. McGraw-Hill, New York.
17. Koeslag, J. H., P. T. Saunders, and J. A. Wessels. 1997. Glucose homeostasis with infinite gain: further lessons from the Daisyworld parable? *J. Endocrinol.* 154:187–192.
18. Saunders, P. T., J. H. Koeslag, and J. A. Wessels. 1998. Integral rein control in physiology. *J. Theor. Biol.* 194:163–173.
19. Yi, T. M., Y. Huang, …, J. Doyle. 2000. Robust perfect adaptation in bacterial chemotaxis through integral feedback control. *Proc. Natl. Acad. Sci. USA.* 97:4649–4653.
20. El-Samad, H., J. P. Goff, and M. Khammash. 2002. Calcium homeostasis and parturient hypocalcemia: an integral feedback perspective. *J. Theor. Biol.* 214:17–29.
21. Ni, X. Y., T. Drengstig, and P. Ruoff. 2009. The control of the controller: molecular mechanisms for robust perfect adaptation and temperature compensation. *Biophys. J.* 97:1244–1253.
22. Ma, W., A. Trusina, …, C. Tang. 2009. Defining network topologies that can achieve biochemical adaptation. *Cell.* 138:760–773.
23. Huang, Y., T. Drengstig, and P. Ruoff. 2012. Integrating fluctuating nitrate uptake and assimilation to robust homeostasis. *Plant Cell Environ.* 35:917–928.
24. Monod, J. 1949. The growth of bacterial cultures. *Annu. Rev. Microbiol.* 3:371–394.
25. Gaudy, Jr., A. F., A. Obayashi, and E. T. Gaudy. 1971. Control of growth rate by initial substrate concentration at values below maximum rate. *Appl. Microbiol.* 22:1041–1047.
26. Thomas, T. D., D. C. Ellwood, and V. M. Longyear. 1979. Change from homo- to heterolactic fermentation by *Streptococcus lactis* resulting from glucose limitation in anaerobic chemostat cultures. *J. Bacteriol.* 138:109–117.
27. Molenaar, D., R. van Berlo, …, B. Teusink. 2009. Shifts in growth strategies reflect tradeoffs in cellular economics. *Mol. Syst. Biol.* 5:323.
28. Kerkeb, L., I. Mukherjee, …, E. L. Connolly. 2008. Iron-induced turnover of the Arabidopsis IRON-REGULATED TRANSPORTER1 metal transporter requires lysine residues. *Plant Physiol.* 146:1964–1973.
29. Felice, M. R., I. De Domenico, …, J. Kaplan. 2005. Post-transcriptional regulation of the yeast high affinity iron transport system. *J. Biol. Chem.* 280:22181–22190.
30. Gitan, R. S., and D. J. Eide. 2000. Zinc-regulated ubiquitin conjugation signals endocytosis of the yeast ZRT1 zinc transporter. *Biochem. J.* 346:329–336.
31. Ooi, C. E., E. Rabinovich, …, R. D. Klausner. 1996. Copper-dependent degradation of the *Saccharomyces cerevisiae* plasma membrane copper transporter Ctr1p in the apparent absence of endocytosis. *EMBO J.* 15:3515–3523.
32. Puig, S., E. Askeland, and D. J. Thiele. 2005. Coordinated remodeling of cellular metabolism during iron deficiency through targeted mRNA degradation. *Cell.* 120:99–110.
33. Rouault, T. A. 2006. The role of iron regulatory proteins in mammalian iron homeostasis and disease. *Nat. Chem. Biol.* 2:406–414.
34. Andrews, N. C., and P. J. Schmidt. 2007. Iron homeostasis. *Annu. Rev. Physiol.* 69:69–85.
35. Rouault, T. A. 2009. Cell biology. An ancient gauge for iron. *Science.* 326:676–677.
36. Salahudeen, A. A., J. W. Thompson, …, R. K. Bruick. 2009. An E3 ligase possessing an iron-responsive hemerythrin domain is a regulator of iron homeostasis. *Science.* 326:722–726.
37. Vashisht, A. A., K. B. Zumbrennen, …, J. A. Wohlschlegel. 2009. Control of iron homeostasis by an iron-regulated ubiquitin ligase. *Science.* 326:718–721.
38. Nemeth, E., M. S. Tuttle, …, J. Kaplan. 2004. Hepcidin regulates cellular iron efflux by binding to ferroportin and inducing its internalization. *Science.* 306:2090–2093.
39. Hentze, M. W., M. U. Muckenthaler, …, C. Camaschella. 2010. Two to tango: regulation of mammalian iron metabolism. *Cell.* 142:24–38.
40. Wu, N., L. Yin, …, M. A. Lazar. 2009. Negative feedback maintenance of heme homeostasis by its receptor, Rev-erbα. *Genes Dev.* 23:2201–2209.
41. Reinking, J., M. M. Lam, …, H. M. Krause. 2005. The *Drosophila* nuclear receptor e75 contains heme and is gas responsive. *Cell.* 122:195–207.
42. Emery, P., and S. M. Reppert. 2004. A rhythmic Ror. *Neuron.* 43: 443–446.
43. Yin, L., and M. A. Lazar. 2005. The orphan nuclear receptor Rev-erbα recruits the N-CoR/histone deacetylase 3 corepressor to regulate the circadian Bmal1 gene. *Mol. Endocrinol.* 19:1452–1459.
44. Yin, L., N. Wu, …, M. A. Lazar. 2007. Rev-erbα, a heme sensor that coordinates metabolic and circadian pathways. *Science.* 318:1786–1789.
45. Radhakrishnan, K., and A. C. Hindmarsh. 1993. Description and Use of LSODE, the Livermore Solver for Ordinary Differential Equations. NASA Reference Publication 1327, Lawrence Livermore National

Laboratory Report UCRL-ID-113855. National Aeronautics and Space Administration, Lewis Research Center, Cleveland, OH.

46. Briat, J.-F., C. Curie, and F. Gaymard. 2007. Iron utilization and metabolism in plants. *Curr. Opin. Plant Biol.* 10:276–282.
47. Walker, E. L., and E. L. Connolly. 2008. Time to pump iron: iron-deficiency-signaling mechanisms of higher plants. *Curr. Opin. Plant Biol.* 11:530–535.
48. Jeong, J., and M. L. Guerinot. 2009. Homing in on iron homeostasis in plants. *Trends Plant Sci.* 14:280–285.
49. Kaplan, C. D., and J. Kaplan. 2009. Iron acquisition and transcriptional regulation. *Chem. Rev.* 109:4536–4552.
50. Yamaguchi-Iwai, Y., R. Stearman, …, R. D. Klausner. 1996. Iron-regulated DNA binding by the AFT1 protein controls the iron regulon in yeast. *EMBO J.* 15:3377–3384.
51. Ueta, R., N. Fujiwara, …, Y. Yamaguchi-Iwai. 2007. Mechanism underlying the iron-dependent nuclear export of the iron-responsive transcription factor Aft1p in *Saccharomyces cerevisiae*. *Mol. Biol. Cell.* 18:2980–2990.
52. Massé, E., and M. Arguin. 2005. Ironing out the problem: new mechanisms of iron homeostasis. *Trends Biochem. Sci.* 30:462–468.
53. Osorio, H., V. Martínez, …, R. Quatrini. 2008. Microbial iron management mechanisms in extremely acidic environments: comparative genomics evidence for diversity and versatility. *BMC Microbiol.* 8:203.
54. Liu, J., A. Sitaram, and C. G. Burd. 2007. Regulation of copper-dependent endocytosis and vacuolar degradation of the yeast copper transporter, Ctr1p, by the Rsp5 ubiquitin ligase. *Traffic.* 8:1375–1384.
55. Wu, X., D. Sinani, …, J. Lee. 2009. Copper transport activity of yeast Ctr1 is down-regulated via its C terminus in response to excess copper. *J. Biol. Chem.* 284:4112–4122.
56. Habener, J. F., B. Kemper, and J. T. Potts, Jr. 1975. Calcium-dependent intracellular degradation of parathyroid hormone: a possible mechanism for the regulation of hormone stores. *Endocrinology.* 97:431–441.
57. LeBoff, M. S., D. Shoback, …, G. Leight. 1985. Regulation of parathyroid hormone release and cytosolic calcium by extracellular calcium in dispersed and cultured bovine and pathological human parathyroid cells. *J. Clin. Invest.* 75:49–57.
58. Russell, J., W. Zhao, …, R. H. Angeletti. 1999. Ca^{2+}-induced increases in steady-state concentrations of intracellular calcium are not required for inhibition of parathyroid hormone secretion. *Mol. Cell Biol. Res. Commun.* 1:221–226.
59. Fujita, T., M. Fukase, …, C. Nakamoto. 1992. New actions of parathyroid hormone through its degradation. *J. Endocrinol. Invest.* 15(9, Suppl 6):121–127.
60. Schmitt, C. P., F. Schaefer, …, O. Mehls. 1996. Control of pulsatile and tonic parathyroid hormone secretion by ionized calcium. *J. Clin. Endocrinol. Metab.* 81:4236–4243.
61. Matsuda, M., T. A. Yamamoto, and M. Hirata. 2006. Ca^{2+}-dependent regulation of calcitonin gene expression by the transcriptional repressor DREAM. *Endocrinology.* 147:4608–4617.
62. Kantham, L., S. J. Quinn, …, E. M. Brown. 2009. The calcium-sensing receptor (CaSR) defends against hypercalcemia independently of its regulation of parathyroid hormone secretion. *Am. J. Physiol. Endocrinol. Metab.* 297:E915–E923.
63. Baylin, S. B., A. L. Bailey, …, G. V. Foster. 1977. Degradation of human calcitonin in human plasmas. *Metabolism.* 26:1345–1354.
64. Semenza, G. L. 2009. Regulation of oxygen homeostasis by hypoxia-inducible factor 1. *Physiology (Bethesda).* 24:97–106.
65. Semenza, G. L., and G. L. Wang. 1992. A nuclear factor induced by hypoxia via de novo protein synthesis binds to the human erythropoietin gene enhancer at a site required for transcriptional activation. *Mol. Cell. Biol.* 12:5447–5454.
66. Semenza, G. L. 2010. Oxygen homeostasis. *Wiley Interdiscip. Rev. Syst. Biol. Med.* 2:336–361.
67. Brand, U., J. C. Fletcher, …, R. Simon. 2000. Dependence of stem cell fate in *Arabidopsis* on a feedback loop regulated by CLV3 activity. *Science.* 289:617–619.
68. Hohm, T., E. Zitzler, and R. Simon. 2010. A dynamic model for stem cell homeostasis and patterning in *Arabidopsis* meristems. *PLoS ONE.* 5:e9189.
69. Gereben, B., A. M. Zavacki, …, A. C. Bianco. 2008. Cellular and molecular basis of deiodinase-regulated thyroid hormone signaling. *Endocr. Rev.* 29:898–938.
70. Braverman, L. E., and U. R. DL, editors. 2004. Werner & Ingbar's The Thyroid: A Fundamental and Clinical Text, 9th ed Lippincott Williams & Wilkins, Philadelphia.
71. Tanaka, K., T. Asami, …, S. Okamoto. 2005. Brassinosteroid homeostasis in Arabidopsis is ensured by feedback expressions of multiple genes involved in its metabolism. *Plant Physiol.* 138:1117–1125.
72. He, J. X., J. M. Gendron, …, Z. Y. Wang. 2005. BZR1 is a transcriptional repressor with dual roles in brassinosteroid homeostasis and growth responses. *Science.* 307:1634–1638.
73. He, J. X., J. M. Gendron, …, Z. Y. Wang. 2002. The GSK3-like kinase BIN2 phosphorylates and destabilizes BZR1, a positive regulator of the brassinosteroid signaling pathway in *Arabidopsis*. *Proc. Natl. Acad. Sci. USA.* 99:10185–10190.
74. Duckworth, W. C., R. G. Bennett, and F. G. Hamel. 1998. Insulin degradation: progress and potential. *Endocr. Rev.* 19:608–624.
75. Gower, B. A., W. M. Granger, …, M. I. Goran. 2002. Contribution of insulin secretion and clearance to glucose-induced insulin concentration in African-American and Caucasian children. *J. Clin. Endocrinol. Metab.* 87:2218–2224.
76. Kakiuchi, S., and H. H. Tomizawa. 1964. Properties of a glucagon-degrading enzyme of beef liver. *J. Biol. Chem.* 239:2160–2164.
77. Yamaguchi, N., K. Koyama, …, J. Imanishi. 1995. A novel proteinase, glucagon-degrading enzyme, secreted by a human pancreatic cancer cell line, HPC-YO. *J. Biochem.* 117:7–10.
78. Gromada, J., W. G. Ding, …, P. Rorsman. 1997. Multisite regulation of insulin secretion by cAMP-increasing agonists: evidence that glucagon-like peptide 1 and glucagon act via distinct receptors. *Pflugers Arch.* 434:515–524.